Predicting discharge capacity Using Machine Learning in Top-Hinged Rectangular Flap gates Measurement

Bahareh Behdarvandi[1], Mohammad Reza Zayeri[2*], Mehdi Ghomeshi[3] and Mehdi Daryaee[4]

1- Phd student in hydraulic structures, Faculty of Water and Environmental Engineering, Shahid Chamran University of Ahvaz, Ahvaz, Iran.
2- Corresponding author Associate professor, Faculty of Water and Environmental Engineering, Shahid Chamran University of Ahvaz, Ahvaz, Iran. (m.zayri@scu.ac.ir)*
3- professor, Faculty of Water and Environmental Engineering, Shahid Chamran University of Ahvaz, Ahvaz, Iran.
4- Associate professor, Faculty of Water and Environmental Engineering, Shahid Chamran University of Ahvaz, Ahvaz, Iran.

ARTICLE INFO

Article history:
Received:
Revised:
Accepted:
Available online:

Keywords: Flap Gate Discharge, Gene Expression Programming (GEP), MARS (Multivariate Adaptive Regression Splines), Machine Learning Models, XGBoost Algorithm.

TO CITE THIS ARTICLE:

Abstract

Accurate prediction of discharge capacity in hydraulic measurement structures is essential for efficient water allocation in irrigation networks. This study evaluates three advanced data-driven models—Multivariate Adaptive Regression Splines (MARS), eXtreme Gradient Boosting (XGBoost), and Gene Expression Programming (GEP)—for estimating the dimensionless discharge capacity ($Q^* = Q/\sqrt{gB^5}$) of rectangular top-hinged flap gates under free-flow conditions. A laboratory dataset comprising 687 experiments from Gorgin and Vatankhah (2022), covering two channel slopes (S = 0 and 0.005), was used. Seven dimensionless variables (h/B, b/B, t/B, L/B, S, θ, and $M/\rho B^3$) were considered as model inputs. The Gamma test identified the optimal input combinations, and the dataset was divided into 75% training and 25% validation subsets while preserving slope-class proportions. SHAP-based sensitivity analysis revealed that the relative upstream flow depth (h/B) is the dominant predictor of Q*, whereas S, b/B, and $M/\rho B^3$ exert secondary but significant effects. Among the models, MARS achieved the highest predictive performance (RMSE = 0.009578, MAE = 0.008161, R^2 = 0.9976), owing to its ability to represent nonlinear hydraulic behavior through piecewise spline functions. XGBoost ranked second (RMSE = 0.02153, R^2 = 0.9877) and exhibited the narrowest 95% prediction uncertainty band, indicating superior robustness for practical applications. Although GEP produced an explicit algebraic equation suitable for engineering calculations, its predictive accuracy was comparatively lower (RMSE = 0.02373, R^2 = 0.985). Comparison with the empirical equations of Gorgin and Vatankhah using the Objective Function (OBF) confirmed that the proposed MARS and XGBoost models outperform previously reported empirical and data-driven approaches for estimating the discharge capacity of rectangular top-hinged flap gates.

Introduction

Accurate measurement of flow discharge is a cornerstone of water resources management, particularly in agricultural irrigation networks where precise water allocation directly determines distribution efficiency and conservation outcomes (Valipour, 2013). Among the hydraulic structures developed for this purpose, top-hinged flap gates have attracted considerable attention owing to their practical advantages: low construction and maintenance costs, passive automatic operation driven by the moment balance between gate weight and hydrodynamic pressure, tolerance for sediment passage, and flexibility for temporary or permanent installation (Salehi and Azimi, 2019). Unlike conventional sluice gates that require external actuation, flap gates self-regulate opening angle in response to upstream head, making them well-suited

for unattended, low-cost flow measurement in irrigation canals.

The hydraulic behaviour of rectangular top-hinged flap gates (RTHGs) has been studied experimentally in the literature. Litrico et al. (2005) derived moment-balance regression equations for the discharge coefficient under free-flow conditions in rectangular cross-sections. Mahmoudi and Farhoudi (2019) used analytical weir and momentum equations to estimate discharge through hinged flaps, reporting average relative errors of 4.41–6.84% depending on gate geometry. Moghtaderi and Valizadegan (2021) proposed a step–discharge relationship for flap gates at the end of trapezoidal channels, achieving an average relative error of 0.22%. Most recently, Gorgin and Vatankhah (2022) conducted a comprehensive laboratory study on RTHGs installed in rectangular channels across two slope conditions and a wide range of gate geometries, producing empirical nonlinear regression equations that serve as the benchmark for the present study.

Despite this experimental foundation, conventional empirical and regression-based formulations for RTHGs share a fundamental limitation: they rely on fixed power-law exponents that cannot adapt to the complex nonlinear interactions among hydraulic variables (upstream head, channel slope) and geometric parameters (gate width, thickness, weight, opening ratio). As discharge transitions from orifice-dominated flow at low head ratios to weir-like behaviour at higher upstream depths, these fixed-form equations introduce systematic prediction errors that undermine operational reliability (Gorgin and Vatankhah, 2022). Machine learning (ML) approaches offer a data-driven alternative capable of capturing such nonlinear relationships without imposing a predetermined functional structure.

Applications of ML to discharge prediction in hydraulic gates and weirs have grown substantially in recent years. Salmasi et al. (2022) compared decision tree and SVM models for inclined sluice gate discharge coefficients under both free and submerged flow. Yan et al. (2023) used convolutional neural networks for rectangular sluice gate discharge prediction, achieving $R^2 > 0.90$ while reducing computational cost. In the context of weirs, Afaridegan et al. (2025) demonstrated the superior performance of hybrid ML models over empirical equations for energy dissipation and discharge prediction in stepped spillways and semi-cylindrical weirs. Bijanvand et al. (2025) and Asgharzadeh-Bonab et al. (2025) reported similar advantages for harmonic plan circular weirs and semicircular labyrinth weirs, respectively.

However, in the specific context of RTHGs, the application of advanced ensemble methods and interpretable ML frameworks remains limited. The study by Behdarvandi et al. (2024) used a restricted set of input parameters and did not incorporate dimensionless analysis, SHAP-based sensitivity interpretation, or formal uncertainty quantification — aspects that are increasingly required for practical deployment. Furthermore, while gradient boosting methods and symbolic regression models have shown strong performance across hydraulic structures, they have not been systematically compared for RTHG discharge prediction.

The present study addresses these gaps by developing and evaluating three complementary data-driven models — Multivariate Adaptive Regression Splines (MARS), eXtreme Gradient Boosting (XGBoost), and Gene Expression Programming (GEP) — for predicting the dimensionless discharge capacity $Q^* = Q/\sqrt{(gB^5)}$ of RTHGs under free-flow conditions. MARS is selected for its piecewise spline structure suited to flow-regime transitions; XGBoost for its robustness to mixed discrete-continuous inputs and resistance to overfitting; and GEP for its ability to produce explicit algebraic equations directly comparable to the empirical formulas of Gorgin and Vatankhah (2022). The Gamma test is used for optimal input selection, SHAP for sensitivity analysis, and confidence-limit-based uncertainty quantification is applied to assess model reliability. The proposed framework provides a more accurate, interpretable, and uncertainty-aware alternative to existing empirical formulations for RTHG discharge prediction.

Materials and Metods

Measuring flow rate channel with a flap gate

The present study employs the laboratory dataset reported by Gorgin and Vatankhah (2022), which constitutes the sole data source for model development and validation. The use of a single, consistently acquired dataset was preferred over combining heterogeneous historical records, as the latter can introduce systematic bias and reduce model generalisability, as documented in comparable hydraulic machine-learning studies (Afaridegan et al., 2025b; Belaabed et al., 2025).

The dataset comprises 687 experimental runs collected under free-flow conditions in a rectangular channel of width B = 0.25 m, covering two bed slope conditions: S = 0 (horizontal, 393 runs) and S = 0.005 (sloping, 294 runs). Gate thickness took primarily two discrete levels, t/B = 0.02 and t/B = 0.04. These quasi-discrete values for S and t/B are noteworthy from a modelling perspective: they preclude the use of continuous regression methods that treat all predictors as smoothly varying, and instead favour tree-based or piecewise approaches capable of detecting threshold effects at fixed parameter levels.

The discharge capacity $Q^* = Q/\sqrt{(gB^5)}$ was selected as the target variable. Seven dimensionless input parameters were identified through dimensional analysis of the governing hydraulic and geometric variables:

$$Q = \phi[h, B, b, S, t, L, g, M, \theta] \quad (1)$$

$$Q^* = \frac{Q}{\sqrt{gB^5}} = \phi\left(\frac{h}{B}, \frac{b}{B}, S, \frac{L}{B}, \frac{t}{B}, \frac{M}{\rho B^3}, \theta\right) \quad (2)$$

In figure (1), Q is the volumetric flow rate (m^3/s), B is the channel width (m), h is the upstream flow depth (m), b is the gate width (m), L is the gate length (m), t is the gate plate thickness (m), S is the channel bed slope (−), θ is the gate opening angle (°), g is gravitational acceleration (m/s^2), and M is the gate mass per unit width (kg/m)

The statistical characteristics of all dimensionless parameters across training and validation subsets are summarised in Table (1). The dataset was partitioned into 75% training (515 runs) and 25% validation (172 runs), with stratified sampling to preserve the proportion of each slope class in both subsets.

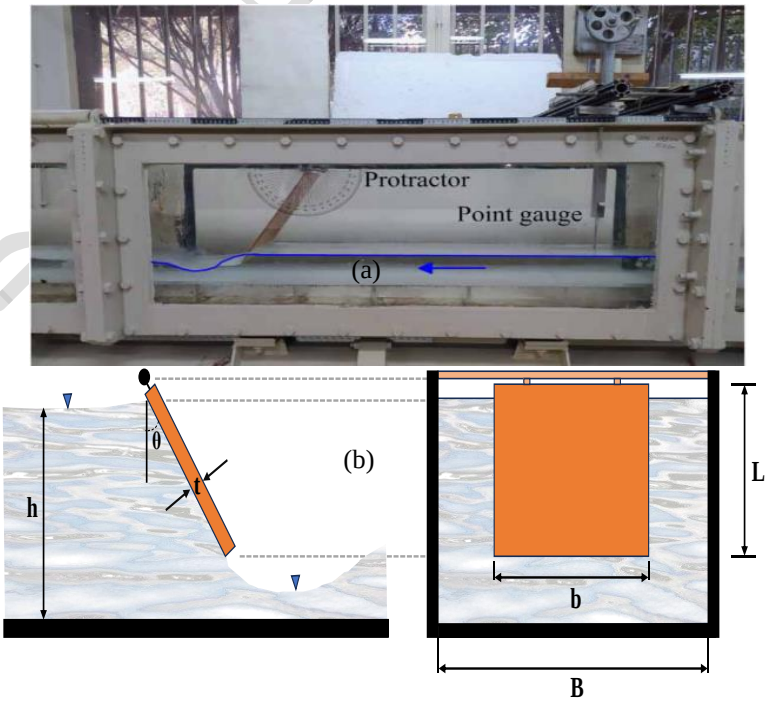


Fig. 1- (a) Schematic of the flow rate measurement channel with a flap gate (Gorgin and Vatankhah, 2022), and (b) Geometric and hydraulic parameters affecting the flow rate.

Table 1- Descriptive Statistics of the Data Allocated in the Training and Validation Stage of Soft Computing Models

Stage	Index	S	θ	$\frac{h}{B}$	$\frac{b}{B}$	$\frac{t}{B}$	$\frac{L}{B}$	$\frac{M}{\rho b^3}$	$\frac{Q}{\sqrt{gB^3}}$
Train	Minimum	0	3.5	0.065	0.2	0.02	0.8	0.029	0.0105
	Maximum	0.005	80	0.951	0.8	0.04	1.2	1.428	0.76
	Average	0.002	42.111	0.408	0.499	0.030	1.009	0.329	0.236
	Standard Deviation	0.002	20.093	0.2209	0.221	0.01	0.2	0.400	0.193
Validation	Minimum	0	3.5	0.0724	0.8	0.02	0.8	0.029	0.011
	Maximum	0.005	81	0.887	0.2	0.04	1.2	1.428	0.736
	Average	0.002	42.401	0.406	0.513	0.0284	1.016	0.289	0.237
	Standard Deviation	0.002	20.510	0.222	0.232	0.01	0.201	0.339	0.195

One-way ANOVA was conducted to evaluate the individual effects of dimensionless parameters on normalized discharge ($\frac{Q}{\sqrt{gB^5}}$) using the complete dataset. Continuous predictors, such as h/B, showed strong linear relationships (R^2 = 0.939, F-statistic = 10,580, p = 0.00), confirming dominant influence. For parameters with discrete levels (S: 0 and 0.005; t/B: primarily 0.02 and 0.04), categorical ANOVA yielded extremely low p-values ($<< 10^{-10}$), indicating significant effects. These results demonstrate that S influences non-uniform acceleration and turbulence beyond velocity head incorporation into upstream depth, while t/B affects gate weight, moment balance, and edge-induced contraction independently of measured θ. The analysis thus supports retaining all parameters as statistically and hydraulically independent, aligning with experimental evidence and ensuring robust dimensional framework for machine learning modeling.

The selection of MARS, XGBoost, and GEP as candidate models in the present study was guided by three interrelated characteristics of the dataset and the hydraulic problem at hand, namely: (i) the nonlinear and regime-transitional nature of RTHG discharge, (ii) the mixed structure of the input parameter space, and (iii) the requirement for practical applicability in field conditions. In summary, the three selected models represent a deliberate methodological progression: from interpretable symbolic equations (GEP) to locally adaptive splines (MARS) to sequential ensemble correction (XGBoost), each addressing a specific limitation of the empirical power-law equations against which they are benchmarked.

GEP model

Gene Expression Programming (GEP) is a synthetic method for resolving genotype systems. Developed by Ferreira (2001), GEP is comparable to genetic algorithms (GA) and genetic programming (GP). GA treats individuals as linear strings of fixed length (chromosomes), while GP treats individuals as non-linear units with different parse tree structures. GEP uses encoded linear strings, or chromosomes, which are represented as non-linear entities. GEP was included specifically to produce an explicit, closed-form algebraic expression for Q* that can be evaluated without computational software — a critical requirement for practical deployment in irrigation field conditions where digital tools may be unavailable. The two main components of GEP are chromosomes and the tree structure (ETS). Translation is the process of decoding the information, which involves a set of rules and codes. In figure (2) presents Algorithm of gene expression programming. GEP has a simple genetic code; the tree illustrates the relationship between the chromosome symbol and the node. The nodes in the trees are determined by GEP rules, which also define the type of interaction in the sub-ETSs. The two main languages on which GEP programming is based are the expression tree language andthe genetic language. This method is classified

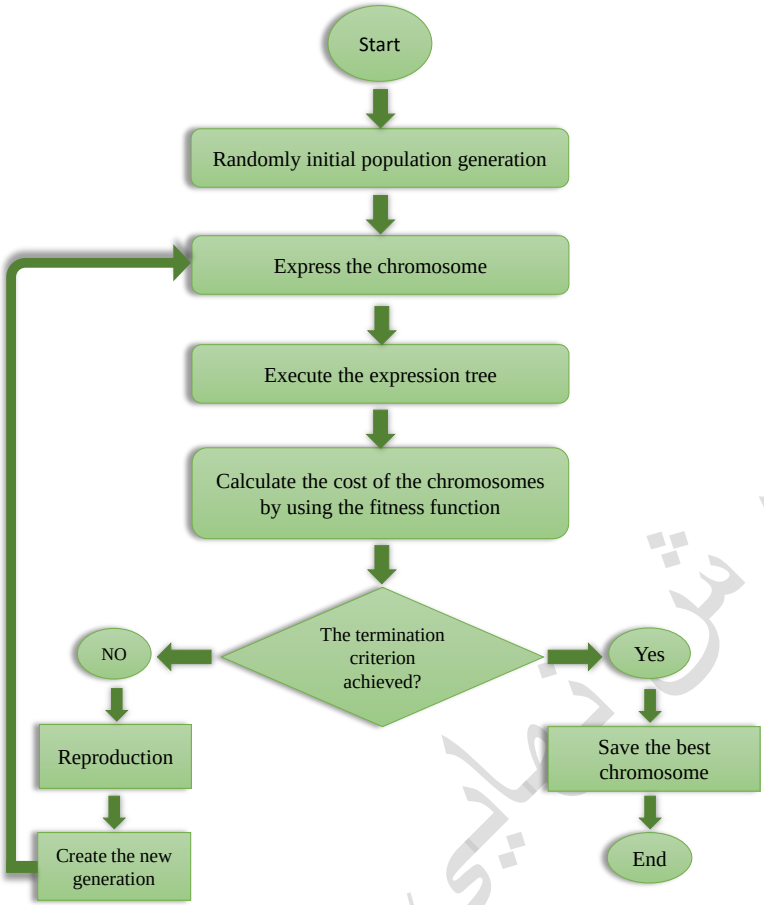


Fig. 2- Algorithm of Gene Expression Programming

among iterative algorithms, all of which are based on Darwin's theory of evolution. These algorithms define a target function in the form of qualitative criteria and then use this function to measure and compare different solution methods through a step-by-step process of correcting data structures, ultimately providing a suitable solution method. Gene programming is the most recent technique among iterative algorithms and has become the most commonly used method due to its sufficient accuracy, with its usage increasing steadily. The main focus of gene programming is on the genetic algorithm, with the distinction that this method uses separate branches instead of bit strings. Each branch consists of a set of terminals (problem variables) and a collection of functions (primary operators).

Multivariate Adaptive Regression Splines (MARS):

MARS, a non-linear and non-parametric method originally introduced by Friedman, models the relationship between sets of input and output variables in a high-dimensional data space using a combination of coefficients and piecewise polynomials (Friedman, 1991). MARS is a non-parametric, non-linear approach for identifying relationships between sets of input and dependent variables in an n-dimensional data space. It does not rely on specific assumptions about the underlying functional relationships among the variables. Instead, MARS employs a divide-and-conquer strategy, dividing the training data into different spline segments with distinct slopes. These segments are separated by "nodes" or endpoints that define the boundaries between different data regions. In this way, the basis functions (piecewise-defined curves) add flexibility to the models, allowing a linear function to incorporate bends, thresholds, and other variations. By combining the basis functions (BFs) and their interactions in a linear manner, the MARS model f(X) can be structured as follows (Zhang, 2020):

$$f(X) = \beta_0 + \sum_{m=1}^{M} B_m \lambda_m(X) \qquad (3)$$

In this context, (λ_m) denotes a basis function, which may be either a single spline or the product of two or more splines. For this study, we have limited the model to a maximum of second-order functions for simplicity, although higher orders may be used if supported by the data. The least squares method is applied to estimate (β), which is a constant, while the basis functions (BFs) are smooth polynomials, specifically splines composed of piecewise linear or cubic functions. A piecewise linear function takes the form max(0, x - t), chosen for simplicity, where (t) serves as a knot. The max(.) function ensures a value of zero unless the positive part is taken.

$$\max(0, x - t) = \begin{cases} x - t & x \geq t \\ 0 & \text{otherwise} \end{cases} \qquad (4)$$

To generate basis functions (BFs), MARS incrementally searches for all variable interactions and potential univariate nodes, selecting them using an adaptive regression algorithm. Creating a MARS model involves a forward phase, in which features are added to identify nodes that improve performance until the maximum predetermined number of terms is reached, resulting in an intentionally overfitted model. This is followed by a backward phase, in which the least effective terms are removed to prevent overfitting.

XGBoost Overview

XGBoost is distinguished by its unique objective function in the learning process. The algorithm provides flexibility in selecting loss functions for model evaluation. Additionally, XGBoost can be applied to both regression and classification tasks. It employs an iterative process that combines multiple weak learners to form a strong predictive model. As shown in Figure (3), the residuals – the differences between the predicted and actual values – are used to refine the previous predictors (i.e. the trees) at each iteration. In regression tasks, the final prediction is obtained by averaging the results of all trees (Han et al., 2019). XGBoost is designed for fast and efficient processing of large datasets and benefits from its block-based computational approach. It also utilises CPU multithreading for parallel processing and continuously improves its algorithm to enhance accuracy. These features make XGBoost a distinctive and powerful model for machine learning.

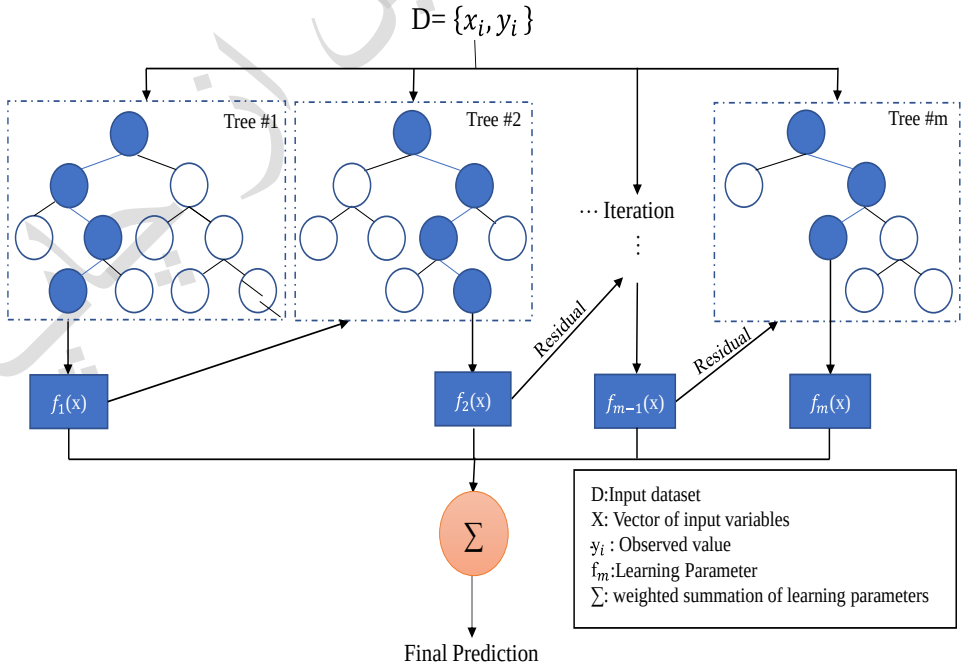


Fig. 3- Flowchart of XGBoost

XGBoost was selected as a complementary ensemble approach for two reasons specific to the structure of the present dataset. First, the dataset contains parameters with quasi-discrete levels — channel slope S takes only two values (0 and 0.005) and gate thickness t/B is concentrated at 0.02 and 0.04 — a feature that tree-based models handle more naturally than regression or neural network approaches, which treat all predictors as continuous. Second, as a gradient boosting algorithm, XGBoost builds predictions sequentially by correcting the residual errors of preceding trees, making it inherently robust to the measurement noise present in laboratory point-gauge and protractor readings.

Wingamma

Gamma Test for Input Selection

As an advanced statistical tool, the gamma test has been used effectively in various fields, including feature selection (Chuzhanova et al., 1998), control theory (Koncar, 1997), communication (De Oliveira, 1999), and modeling (Hassan et al., 2015; Moghaddamnia et al., 2009; Piri et al., 2009; Remesan et al., 2009 & 2008; Shamim et al., 2015). This test estimates the mean squared error (MSE) by modelling the complex relationships between specific inputs and outputs. The underlying principle of the algorithm is that a given output (y) is a function of a given input (x). This function can be divided into two components: one representing the smooth part of the function and the other accounting for the noise in the data. If we denote the smooth function as f and define r as the part of the output that cannot be captured by any smooth model, the relationship between y and x can be expressed mathematically as follows (Agalbjorn et al., 1997):

$$Y = f(x) + r \tag{5}$$

The mean value of r is assumed to be zero by assigning a constant error to the unknown function f. Although f is unknown, the gamma test enables the estimation of r under certain conditions. As the number of observations increases, the gamma value converges to an asymptotic value, representing the variance of the noise in the output (Stefánsson et al., 1997).This process quantifies the proportion of variance in the output that cannot be explained by a smooth data model. Additionally, the calculated gamma values are often used as mean squared error (MSE) targets for model training.

SHAP (SHapley Additive exPlanations)

SHAP is a model-agnostic method for interpreting predictions from any machine learning model (Lundberg and Lee, 2017). It applies game theory and local explanations to allocate each feature's contribution to the final prediction based on its marginal effects (Parsa et al., 2020). To ensure a fair distribution of feature contributions, the SHAP values are calculated using equation (6):

$$\phi_i = \sum_{S \subseteq N \setminus \{i\}} \frac{|S|!\,(n - |S| - 1)!}{n!} [v_x(S \cup i) - v_x(S)] \tag{6}$$

Here, $\phi_i(v)$ represents the contribution of feature i, N is the set of all features in the model, and n denotes the total number of features. S is a subset of features excluding i, while $v_x(S)$ is the expected prediction for a given subset S. The term $[v_x(S \cup i) - v_x(S)]$ captures the change in prediction due to feature i. In this study, the SHAP values were calculated using the 'shap' library in Python.

Results and Discussion

Investigation of the distribution of dimensionless variables

Figure (4) presents the dispersion and density matrix of the input and target variables used for correlation analysis. The results show that θ and h/B have the strongest positive correlations with the target variable (r = 0.91 and r = 0.97), followed by b/B (r = 0.70). In contrast, S, t/B, and L/B exhibit negligible correlations ($r \approx -0.05$ to 0.05). the high correlation of h/B with Q* reflects the dominant role of upstream head in controlling the flow energy, consistent with gate hydraulic theory. The negligible correlation of L/B and t/B suggests these are secondary geometric modifiers. The density

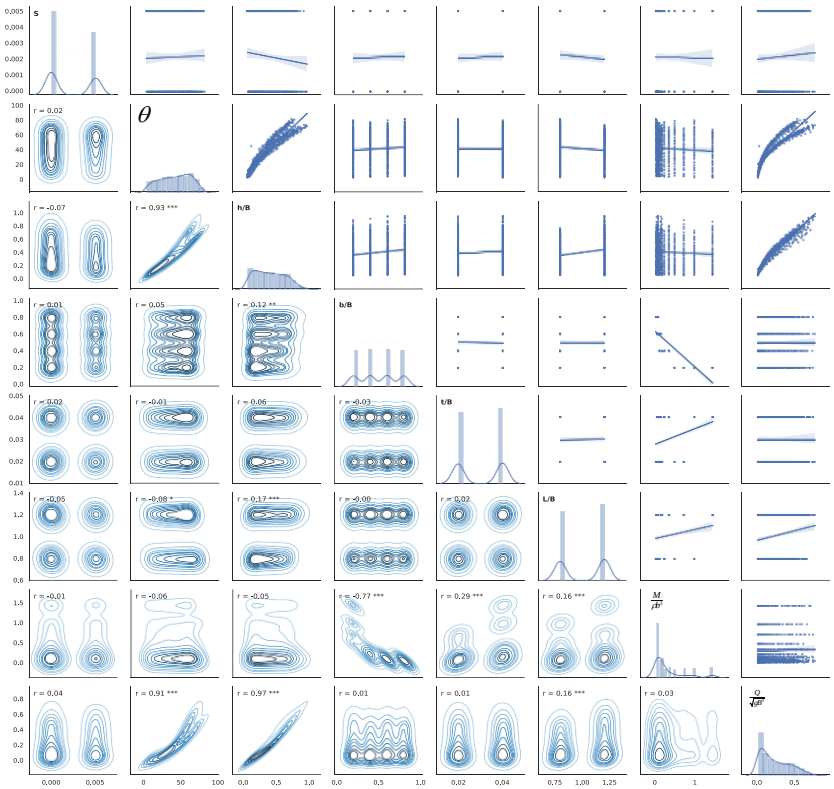


Fig. 4-Distribution Diagram of Dimensionless Variables

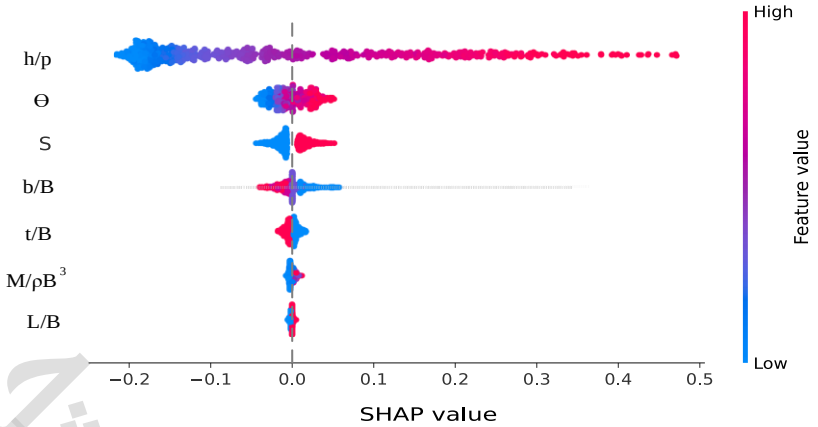


Fig. 5-Shap Analysis Results

plot of the target variable indicates data concentration in the lower range with slight deviation from normality, which favours nonlinear models such as MARS and XGBoost. Overall, θ, h/B, and b/B are key predictors for model development and optimisation.

Sensitivity Analysis Results

According to Figure (5), the sensitivity analysis using the SHAP method is presented. As shown, the variable h/B has the greatest effect as an input parameter in predicting the discharge capacity,($\frac{Q}{\sqrt{gB^5}}$). It is also observed that higher values of this parameter (red dots) increase the discharge capacity. The least effective parameter, according to the figure, is L/B. For the parameters θ and S, similar to h/B, higher values increase the dimensionless flow rate, while lower values also lead to an increase in the dimensionless discharge.

The Gamma Test was applied to systematically identify the optimal combination of dimensionless input parameters for predicting Q*. A total of 127 plausible input combinations were generated from the seven candidate dimensionless parameters (S, h/B, b/B, t/B, L/B, θ, $M/\rho B^3$), and the Gamma statistic was computed for each. The resulting variation in Γ across all combinations is illustrated in Figure (6). Based on the minimum gamma criterion, seven combinations were identified as optimal — defined here as those yielding Γ values in the lowest 5.5% of the distribution — and retained for model development. This selection criterion ensures that the constructed models operate on input subsets with the highest achievable signal-to-noise ratio, thereby promoting smoothness, generalisability, and resistance to overfitting.

The seven selected combinations and their corresponding Γ values are listed in Table (2). Model 1, with Γ = 0.000102, achieves the lowest gamma value among all 127 combinations, indicating that the input subset {S, h/B, b/B, t/B, $M/\rho B^3$} provides the most informative and smooth mapping to Q*. Physically, this result is consistent with the ANOVA findings reported in Section 2.1: the parameters retained in Model 1 collectively capture the dominant hydraulic mechanisms governing RTHG discharge — upstream energy head (h/B), gate geometry and weight (b/B, t/B, $M/\rho B^3$), and slope-induced acceleration effects (S) — while excluding L/B and θ, whose independent contributions to Q* are largely redundant given their high collinearity with h/B (r = 0.91 for θ, as shown in Figure 4). As Γ increases from Model 1 to Model 7 (Γ = 0.001039), the input combinations progressively omit one or more of these physically significant parameters, resulting in a larger irreducible prediction error. The Γ values in Table 2 thus serve a dual purpose: as a model selection criterion during training, and as an upper-bound estimate of the minimum achievable MSE against which final model errors can be benchmarked during validation.

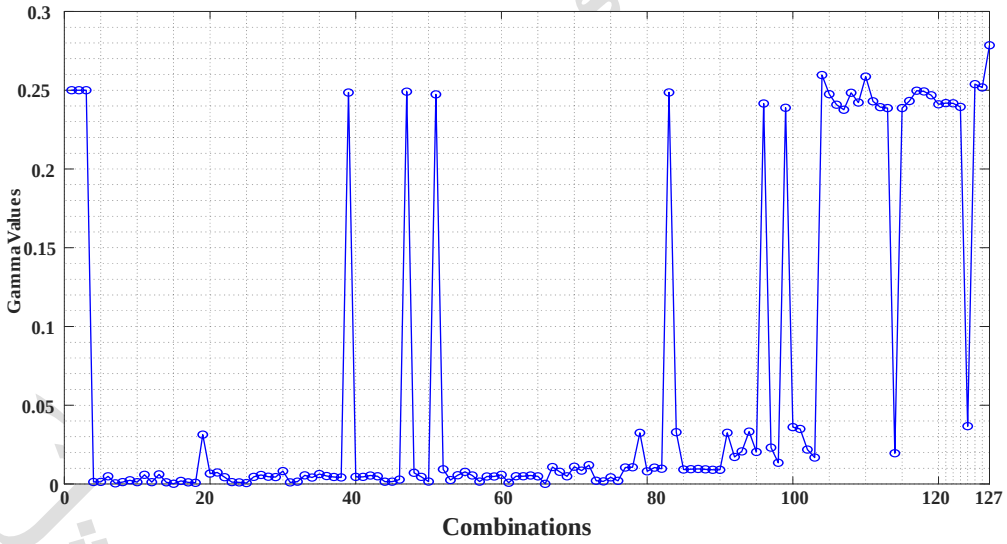


Fig. 6- Variation of gamma values with respect to combinations

Table 2- Selected combinations with minimum gamma values

Model	Expression	Gamma values
Model 1	$\frac{Q}{\sqrt{gB^5}}=\phi\left(\frac{h}{B},\frac{b}{B},S,\frac{L}{B},\frac{M}{\rho B^3},\theta\right)$	0.00010235
Model 2	$\frac{Q}{\sqrt{gB^5}}=\phi\left(\frac{h}{B},S,\frac{L}{B},\frac{t}{B},\frac{M}{\rho B^3},\theta\right)$	0.000153357
Model 3	$\frac{Q}{\sqrt{gB^5}}=\phi\left(\frac{h}{B},S,\frac{L}{B},\frac{t}{B},\frac{M}{\rho B^3}\right)$	0.000413698
Model 4	$\frac{Q}{\sqrt{gB^5}}=\phi\left(\frac{h}{B},\frac{b}{B},S,\frac{L}{B},\theta\right)$	0.000611591
Model 5	$\frac{Q}{\sqrt{gB^5}}=\phi\left(\frac{h}{B},S,\frac{t}{B},\frac{M}{\rho B^3},\theta\right)$	0.000745721
Model 6	$\frac{Q}{\sqrt{gB^5}}=\phi\left(\frac{h}{B},S,\frac{L}{B},\frac{M}{\rho B^3},\theta\right)$	0.00103402
Model 7	$\frac{Q}{\sqrt{gB^5}}=\phi\left(\frac{h}{B},\frac{b}{B},S,\frac{t}{B},\frac{M}{\rho B^3}\right)$	0.001039314

Development of Artificial Intelligence Models

Development of the GEP model

The GEP model was first assembled using one gene with two head lengths. In successive runs, one gene and one head length were added, step by step. Performance on the training data and the test data stayed largely unchanged after the number of head lengths reached eight and the chromosome contained three genes. The settings were therefore fixed at a head length of 8 with three genes per chromosome. A multiplication operator was used to connect the three genes.

After 208649 generations, the value of the fitness function and the coefficient of determination for both datasets showed no meaningful change, which suggested that further evolution was unnecessary. Table 3 reports the general settings, the fitness function, the program structure, the numerical constants, and the genetic operators applied in building the GEP models for all combinations in the table (3). All parameters were selected by trial and error, with the aim of obtaining a usable algebraic form that links the output variable to the input variables, consistent with standard GEP practice (Ferreira, 2006, 2001).

The function set applied during model development included addition, subtraction, multiplication, and division. It also contained square root, cube root, fourth root, and fifth root operations. Inverse and negation were allowed, along with powers of the input variable up to the fifth order. Multi-input operators were included as well, namely Add3, Add4, Sub3, Sub4, Mul3, and Mul4. Seven different GEP scenarios were developed and compared using several statistical indices according figure (7). Among these, Scenario 7 showed the best performance, with the lowest RMSE (0.02373) and MAE (0.01854), and the highest coefficient of determination (R^2 = 0.985). Additional metrics, including SRMSE (0.1002), correlation coefficient (CC = 0.9933), Kling–Gupta Efficiency (KGE = 0.9575), and PBIAS (−2.489), confirmed the model's stability and minimal bias. The corresponding expression tree (ET), together with its three sub expression trees, is shown in Figure (7). The symbols d0, d1, d2, d3, and d4 refer to the nondimensional variables S, $\frac{h}{B}$, $\frac{b}{B}$, $\frac{t}{B}$ and $\frac{M}{\rho B^3}$ respectively. Figure (7a) presents the numerical constant assigned to the first gene, where c8 takes the value 1.27. The second gene is different. It contains no numerical constants at all, as illustrated in Figure (7b). Figure (7c) relates to the third gene. In this case, the constant c2 was calculated as 2.595. From this configuration, Eq. (7) was obtained for estimating the discharge capacity of rectangular flap gates.

Table 3- Applied settings of the developed GEP model.

Category	Parameters	Values
General settings	Number of chromosomes	30
General settings	Number of genes	3
General settings	Head size	8
General settings	Tail size	25
General settings	Dc size	25
General settings	Gene size	58
General settings	Linking function	Multiplication
Fitness	Function	RMSE (Root Mean Square Error)
Program Structure	Program size	40
Program Structure	Literals	42
Program Structure	Used variables	$\frac{h}{B}, \frac{b}{B}, S, \frac{L}{B}, \frac{M}{\rho B^3}, \theta$
Numerical Constants	Data type	Floating-point
Numerical Constants	Constants per gene	10
Numerical Constants	Upper bound	10
Numerical Constants	Lower bound	-10
Genetic operators	Mutation	Optimal evolution
Genetic operators	Inversion	0.00138
Genetic operators	Gene recombination/transposition rate (1-point and 2-point)	0.00546
Genetic operators	Insertion sequence (IS) transposition	0.00277

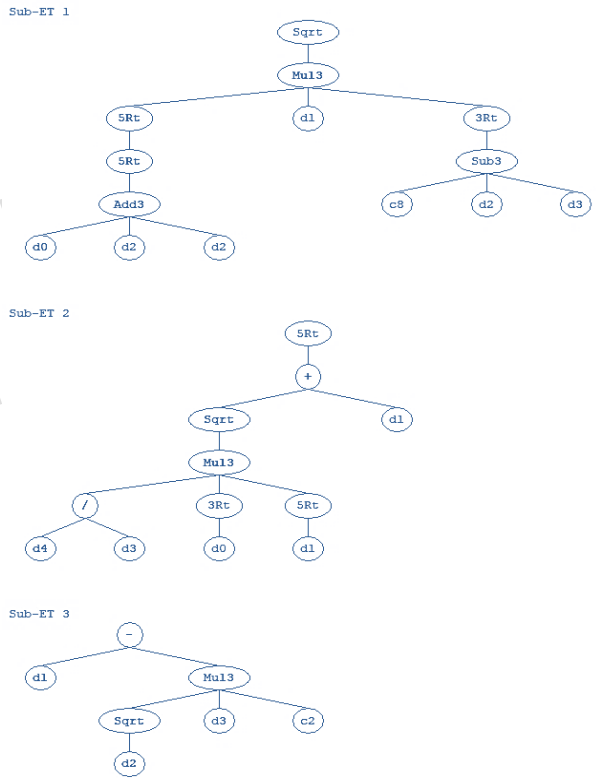


Fig. 7-sub-expression trees (ET) of the developed GEP model (a) sub-ET 1, (b) sub-ET 2, and (c) sub-ET 3.

The expression is written below. The analytical expression derived from the optimal GEP configuration (table 3) clearly captures the nonlinear dependency between $\frac{Q}{\sqrt{gB^5}}$ and the key dimensionless parameters

$$\frac{Q}{\sqrt{gB^5}} = \sqrt{\sqrt[5]{\sqrt[5]{\left(S+2\frac{b}{B}\right)}\times\frac{h}{B}\times\sqrt[3]{\left(1.27-\frac{b}{B}-\frac{t}{B}\right)}}} \times \sqrt[5]{\sqrt{\left(\frac{\frac{M}{\rho B^3}}{\frac{t}{B}}+\frac{h}{B}\right)\times\left(\sqrt[3]{S}\right)\times\sqrt[5]{\frac{h}{B}}+\frac{h}{B}} \times\left(\frac{h}{B}-\left(\sqrt{\frac{b}{B}}\times\frac{t}{B}\times 2.595\right)\right)} \quad (7)$$

Unlike MARS or XGBoost, whose predictions are computed through matrix operations or ensemble voting, GEP outputs a human-readable formula (Equation 7) directly comparable to the empirical equations of Gorgin and Vatankhah (2022). This allows a rigorous quantitative assessment of how much predictive accuracy is gained by transitioning from physically derived regression to evolved symbolic regression, and ultimately to flexible spline or boosting models. Figure 8 presents the comparative performance of seven GEP scenarios across multiple statistical indices (RMSE, MAE, R^2, CC, KGE, PBIAS). As shown in Figure (8), Scenario 7 consistently achieves the best performance across all indices, recording the lowest RMSE (0.02373) and MAE (0.01854), the highest R^2 (0.985) and CC (0.9933), a KGE of 0.9575 confirming minimal bias and variance error, and a PBIAS of −2.489% indicating negligible systematic underestimation. Scenarios 1 through 6 show progressively degraded performance as input combinations deviate from the optimal subset identified by the minimum Gamma criterion, with RMSE increasing monotonically from Scenario 7 toward Scenario 1. This trend is physically consistent: scenarios omitting h/B or S lose the two hydraulically dominant predictors confirmed by SHAP analysis Figure (5) and ANOVA results, leading to higher residuals particularly at low and peak discharge values where these parameters govern flow regime transitions most strongly. Based on this analysis, Scenario 7 was selected as the final GEP configuration for all subsequent comparisons and uncertainty analysis.

Figure (9) presents a three-panel graphical assessment of the optimal GEP model (Scenario 7) on the training and validation datasets. Panel (a) shows a scatter plot of observed versus predicted Q* values against the 45° reference line, together with ±10% error bounds. The close clustering of data points along the 45° line, with the majority falling within the ±10% error bounds in both training and validation stages, confirms the absence of systematic over- or under-prediction across the full operating range of Q*. Panel (b) shows the time-series comparison of observed and predicted Q* values across all runs, demonstrating consistent tracking of discharge fluctuations without phase lag or amplitude distortion. Panel (c) presents the distribution of prediction residuals (Q*_observed − Q*_predicted), which follows an approximately normal distribution centred near zero. The near-zero mean of the residual distribution confirms the absence of systematic bias in the GEP predictions, while the spread of the distribution reflects the inherent variability associated with laboratory measurement uncertainty in point-gauge readings at low h/B values. Overall, the GEP model proved to be a powerful and interpretable soft computing approach for accurately modelling discharge behaviour in rectangular top-hinged flap gates.

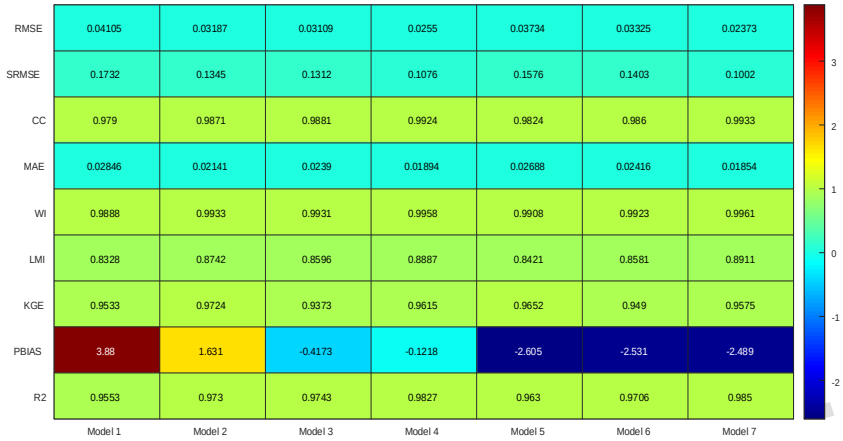


Fig. 8- Performance Results of the GEP Model for Different Scenarios

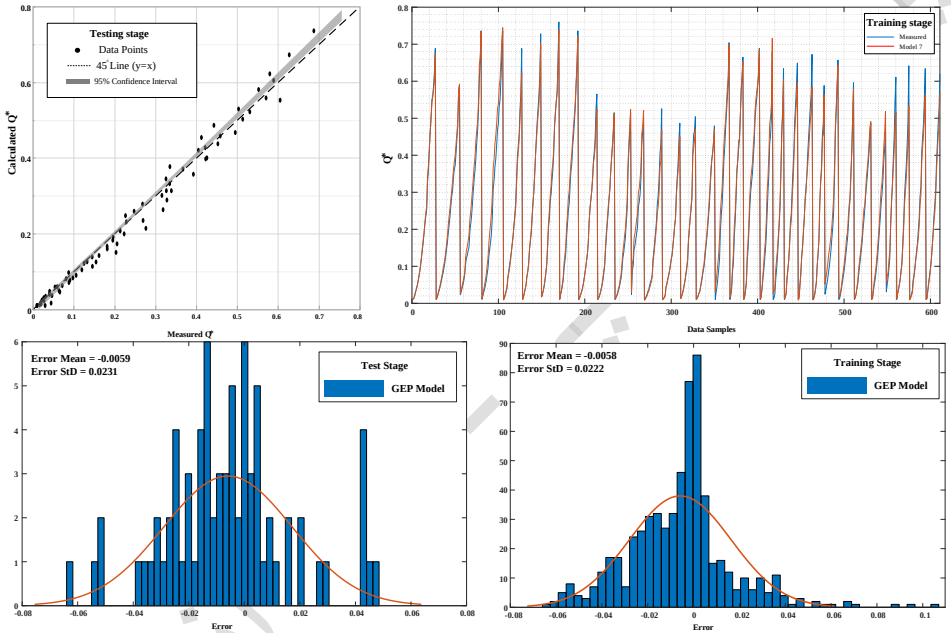


Fig. 9-Results of the GEP Model Developed in the Training and Validation Phase

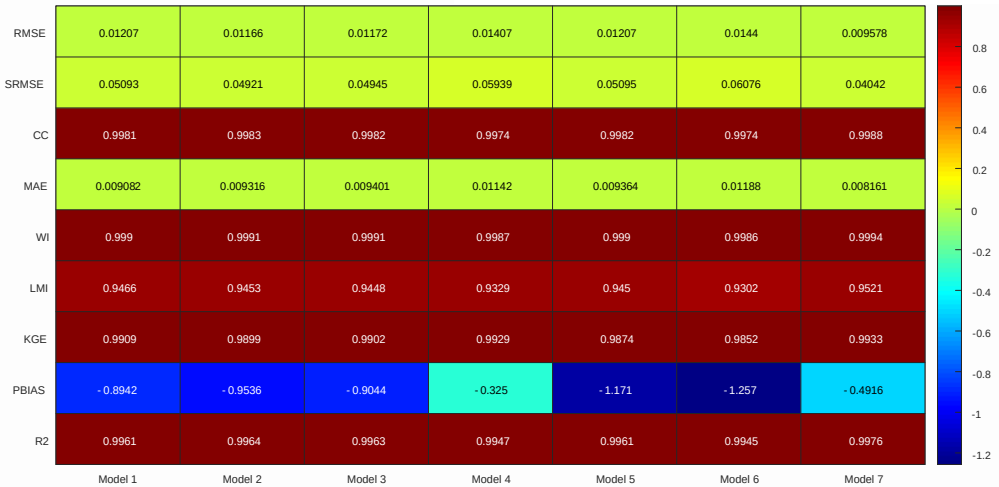


Fig. 10-Performance Results of the MARS Model for Different Scenarios

Table 4-Base Functions and Values (β_M) in the Mars model

(β_M)	Base Functions
0.643	BF1 = max(0, b/B -0.3328)
-0.294	BF2 = max(0,0.3328 -b/B)
18.847	BF3 = max(0, h/B +0)
-0.309	BF4 = max(0, S -0.6)
0.297	BF5 = max(0,0.6 -S)
-0.627	BF6 = BF5 * max(0,0.6576 -b/B)
-17.360	BF7 = BF3 * max(0, S -0.4)
32.438	BF8 = BF3 * max(0,0.4 -S)
0.362	BF9 = max(0, b/B -0.5708)
0.820	BF10 = max(0,0.04 -t/B) * max(0, b/B -0.1676)
-6.286	BF11 = max(0,0.04 -t/B) * max(0,0.1676 -b/B)
-196.663	BF12 = BF3 * max(0, t/B -0.02)
1.220	BF13 = BF4 * max(0, b/B -0.8628)
0.480	BF14 = BF4 * max(0,0.8628 -b/B)
0.237	BF15 = max(0,0.1656 -b/B)
-1.230	BF16 = max(0, b/B -0.1656) * max(0, M/rB3 -0.18061122)
1.806	BF17 = max(0, b/B -0.1656) * max(0,0.18061122 -M/rB3)
1.171	BF18 = max(0, b/B -0.1656) * max(0, M/rB3 -0.07843242)
-34.420	BF19 = max(0,0.5708 -b/B) * max(0, h/B +0)

Development of the MARS model

The performance of the MARS (Multivariate Adaptive Regression Splines) model was evaluated using multiple statistical indicators, including RMSE, MAE, SRMSE, CC, KGE, WI, LMI, PBIAS, and R^2. As shown in Figure (10), Scenario 7 achieved superior accuracy, recording the lowest RMSE= 0.009578 and MAE= 0.008161, and the highest CC= 0.9888 and R^2 = 0.9976. Other indices also confirmed its stable and precise performance. These results demonstrate the strong flexibility of the MARS algorithm in modeling nonlinear relationships and highlight Scenario 7 as the most accurate and reliable configuration for predicting the target variable.

During the development of the MARS (Multivariate Adaptive Regression Splines) model, 25 basis functions were initially generated in the model construction phase. In the subsequent pruning stage, six of these functions were eliminated to prevent overfitting and improve model generalisation. Consequently, an optimal MARS model comprising 19 effective basis functions was obtained. The general mathematical form of the final model is presented in Equation (8), while the detailed formulation of the developed basis functions is summarised in Table (4).

$$Q^* = 0.083 + \sum_{M=1}^{19} \beta_M BF_M(x) \quad (8)$$

The performance of the optimal MARS model (Scenario 7) was evaluated using both training and testing datasets, as shown in Figure (11). The close alignment of observed and predicted Q^* values along the 45° line (R^2 = 0.9981) and the slope of 1.015 confirm the model's high accuracy during training. The time-series plot also demonstrates an excellent match between actual and simulated data. Error analysis indicates unbiased and stable performance, with a mean error of 9.65×10^{-17} and a standard deviation of 0.0118 in training, and 0.00161 and 0.00793 in testing, respectively. The concentration of residuals around zero and their near-normal distribution highlight the model's strong generalisation ability, validating MARS as an effective predictive tool for discharge capacity estimation. These characteristics motivated the selection of MARS as the primary candidate model. The piecewise spline architecture of MARS is specifically designed to identify and represent regime-transition thresholds through adaptive knot placement, without requiring the modeller to prespecify the location or number of breakpoints. Each basis function in the final MARS model Table (4) corresponds directly to a physically

meaningful sub-range of the input space — for example, BF7 and BF8 capture the differential effect of slope at a critical h/B threshold of 0.4, while BF12 represents the interaction between upstream head and gate thickness. This interpretability makes MARS directly comparable to analytical formulations while retaining the flexibility of a data-driven model.

From a hydraulic perspective, MARS's superior performance stems from its piecewise linear spline structure, which effectively approximates the abrupt transitions in flow regime caused by vena contracta intensification and flow separation at larger gate openings. As upstream head ratio (h/B) increases, the contraction coefficient rises nonlinearly due to reduced edge effects and smoother flow detachment similar to observations in Nejatipour et al. (2025).

The 19 retained basis functions Table (3) explicitly incorporate interactions involving h/B, channel slope (S), and relative gate thickness (t/B), allowing the model to accurately represent the shift from orifice-like to weir-like behavior at critical h/B thresholds. This explains the minimal scatter at peak discharges, where turbulence and recirculation zones are most pronounced.

XGBoost Model Development

The XGBoost model was applied to predict discharge in hydraulic structures. Seven scenarios were evaluated using RMSE, MAE, R^2, CC, KGE, WI, LMI, and PBIAS (Figure 12). Scenario 1 was identified as the optimal configuration, achieving RMSE = 0.02153, MAE = 0.01495, and R^2 = 0.9877. The model also exhibited a CC of 0.9944, KGE of 0.9611, and PBIAS of 1.753, demonstrating high accuracy, stability, and minimal bias. These results confirm that the XGBoost model is a reliable and effective tool for predicting discharge in hydraulic engineering applications.

Figure (13) shows strong agreement between the observed and predicted values, with the XGBoost model outputs closely matching the actual data during training. The normally distributed residuals with a near-zero mean indicate unbiased and stable performance. As a boosted decision tree algorithm, XGBoost effectively models nonlinear relationships, handles complex datasets, and resists overfitting. Its cumulative structure, in which new trees iteratively correct previous errors, enhances both accuracy and robustness. The model's tunable hyperparameters (e.g., learning rate, tree depth, and number of trees) allow precise optimisation. Although XGBoost demonstrated excellent predictive capability and generalisation, comparison with the optimal MARS model (Scenario 7) indicated that MARS achieved higher accuracy, with lower RMSE (0.00578), lower MAE (0.008181), and higher R^2 = 0.9978 in estimating the discharge capacity

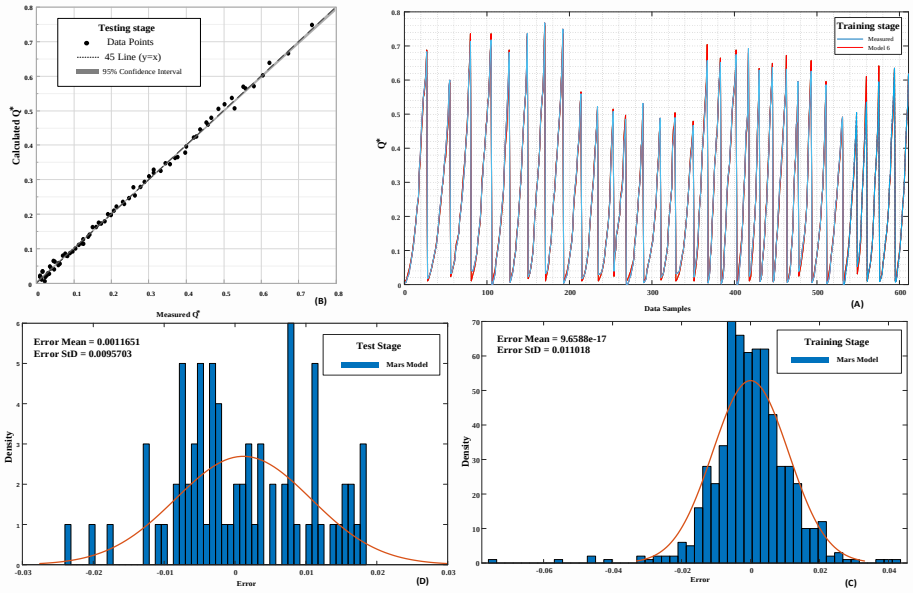


Fig. 11- Results of the MARS model developed in the training and validation phase

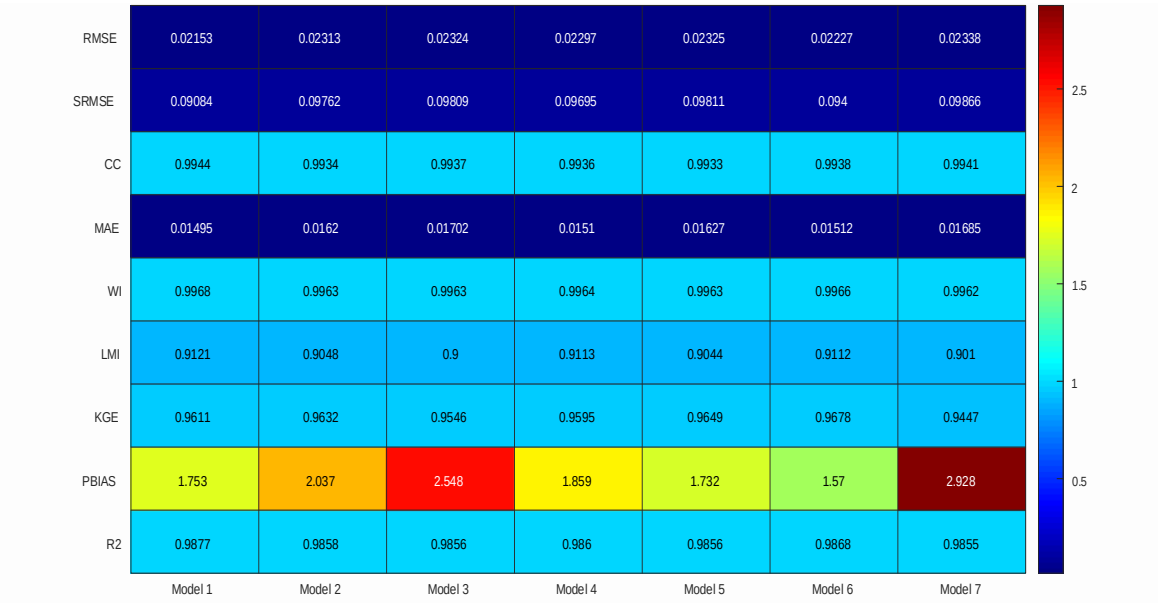


Fig. 12-XGBoost model performance results for different scenarios

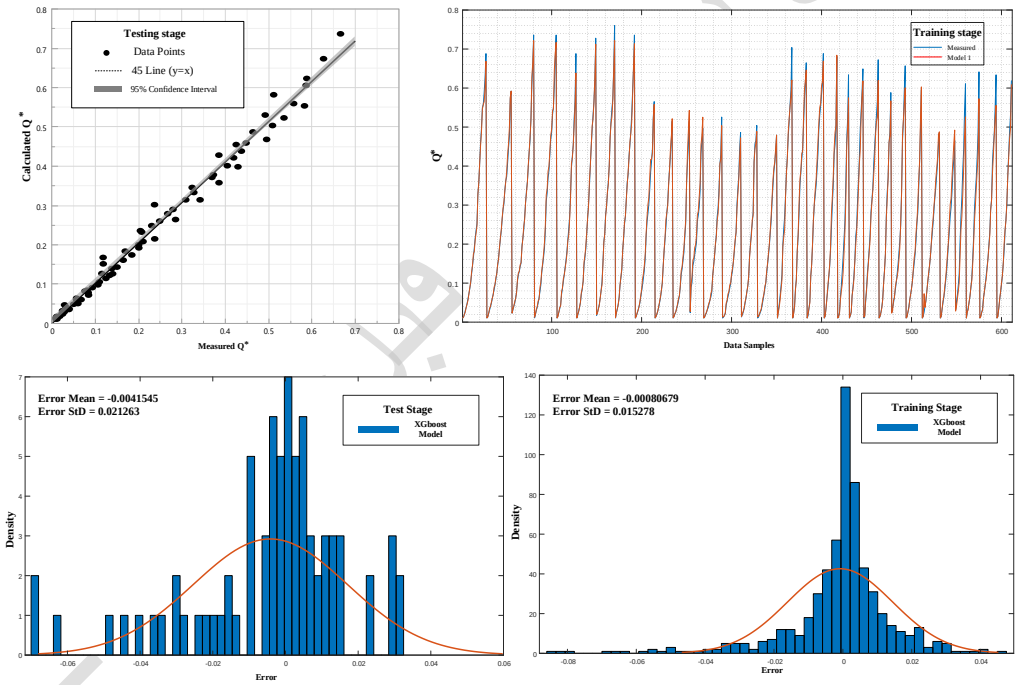


Fig. 13-Results of the XGBoost Model Developed in the Training and Validation Phase

Hydraulically, XGBoost's tree-boosting architecture excels at sequential error correction, effectively modeling the progressive influence of dominant parameters such as h/B (most important per SHAP analysis) and channel slope S. At low Q*, the flow is dominated by partial gate opening and strong vena contracta effects, leading to higher relative measurement uncertainty in laboratory data; XGBoost's regularization helps mitigate this, but residual overestimation may reflect minor overfitting to majority mid-range patterns. At peak discharges, intensified flow separation and downstream hydraulic jumps Nejatipour et al. (2025) introduce turbulence-driven variability that challenges even ensemble methods, explaining the subtle underprediction. Overall, XGBoost's cumulative learning process provides high robustness to abrupt changes in discharge induced by varying upstream head.

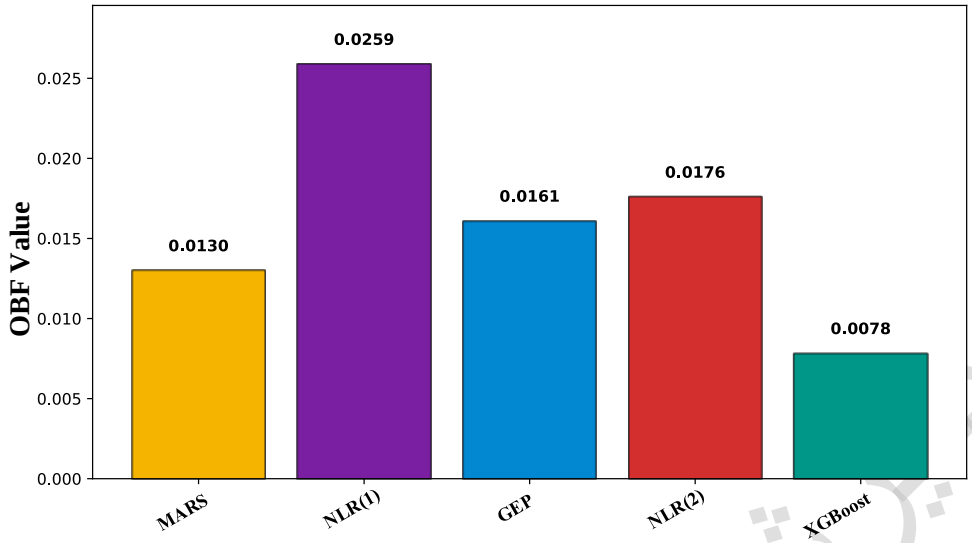


Fig. 14-The values of OBF values for the proposed data-driven models for the prediction of discharge capacity compare regression-based equations.

Comparison with Previous Studies

The recently proposed regression-based equations by Goegin and Vatankhah (2022) for the prediction of discharge capacity in Flap gates are listed in Equations (9) and (10). The previous study by Behdarvandi et al. (2024) provided the results of Support Vector Machine (SVM), Random Forest (RF) and GMDH algorithms for training and testing datasets. For comparison of the previously suggested datadriven results with the outcomes of MARS, GEP and XGBoost provided in this study, the taylor diagram and the objective function (OBF) criterion is used. The OBF criterion is defined as equation (11).

$$\text{NLR (1)}\quad \frac{Q}{\sqrt{gB^5}} = (0.547 - 36S)\left(\frac{h}{B}\right)^{1.82-8S} \times \left(\frac{b}{B}\right)^{-0.13-40S}\left(\frac{t}{B}\right)^{-0.12-23.3S}\left(\frac{L}{B}\right)^{-0.1} \quad (9)$$

$$\text{NLR (2)}\quad \frac{Q}{\sqrt{gB^5}} = (0.3 - 30S)\left(\frac{h}{B}\right)^{1.67-23S} \times \left(\frac{b}{B}\right)^{-0.13-34S}\left(\frac{t}{B}\right)^{-0.09-22.2S}\theta^{0.152+14S} \quad (10)$$

$$\text{OBF} = \left(\frac{n_{train}}{n_{all}} \times \frac{RMSE_{train} + MAE_{train}}{R^2_{train} + 1}\right) + \left(\frac{n_{test}}{n_{all}} \times \frac{RMSE_{test} + MAE_{test}}{R^2_{test} + 1}\right) \quad (11)$$

where $n_{training}$ data, $n_{testing}$ data, and n_{all} data refer to the number of training samples, testing, and total datasets. The best optimal approach reaches the lowest value of the OBF criterion. As observed in Equation (11), the OBF criterion simultaneously considered the R^2, RMSE, and MAE values for both the training and testing datasets. the values of OBF for the proposed data-driven models are calculated and displayed in Figure (14).

As observed in Figure (14), the values of the OBF criterion for the Xgboost and Mars models have minimum values compared to NLR(1), NLR(2), and GEP methods. In addition, the Xgboost model has the lowest value of OBF (0.0078) compared to other models, confirming the best performance of Xgboost for the estimation of discharge capacity. From a hydraulic standpoint, the discharge capacity Q* does not respond linearly to changes in the input parameters. At low upstream head ratios (h/B < 0.2), the flow beneath the gate is dominated by orifice-like contraction with a pronounced vena contracta, in which the discharge scales approximately with $(h/B)^{0.5}$. As h/B increases, the vena contracta diminishes, the contraction coefficient rises nonlinearly, and the flow transitions toward weir-like behaviour with a steeper h/B exponent. This piecewise, regime-dependent behaviour — which is also modulated by channel slope (S) and gate thickness (t/B) — cannot be captured by the fixed-exponent power-law formulations of Gorgin and Vatankhah (2022), (Equations 9 and 10), which implicitly assume a single flow regime across

the entire operating range. Furthermore, the ANOVA results presented in Section 2.1 confirm that S and t/B exert statistically independent effects on Q* beyond their contribution through θ alone, implying multiplicative interaction terms of the form S × h/B and t/B × b/B that fixed-form regression equations are structurally unable to represent.

The Taylor diagram simultaneously represents correlation, standard deviation, and centered RMS error, allowing a comprehensive assessment of model accuracy. According to the plotted results in figure (15), XGBoost is positioned closest to the reference point, showing the highest correlation and lowest deviation among all models. This indicates that XGBoost provides the most accurate and stable predictions of discharge capacity. Following XGBoost, the MARS model demonstrates relatively strong performance, while GMDH and RF exhibit moderate accuracy. The GEP model performs acceptably but not as well as XGBoost or MARS. In summary, based on the Taylor diagram, XGBoost outperforms all other models in predicting discharge capacity.

The GEP model produced explicit analytical expressions (Equation 7) but comparatively lower accuracy, with higher error metrics than MARS and. Despite this, it maintained acceptable performance and valuable interpretability.

From a hydraulic viewpoint, GEP's symbolic regression approach successfully encodes physically meaningful terms involving h/B, b/B, and S (visible in sub-expression trees, Figure 7), aligning with theory that upstream head ratio governs contraction coefficient and discharge scaling. However, the increased scatter at intermediate and peak discharges arises from GEP's difficulty in fully representing the complex, non-smooth transitions driven by flow separation, recirculation zones, and edge-induced turbulence (Nejatipour et al., 2025). These phenomena generate discontinuous behavioral shifts that symbolic forms struggle to capture as precisely as spline (MARS) or iterative boosting (XGBoost) methods. Consequently, while GEP offers transparent equations suitable for hand calculations, its predictive fidelity is lower in regions of pronounced vena contracta and energy dissipation variability.

Uncertainty analysis.

To evaluate the level of uncertainty in the proposed models, we calculate the confidence limits of prediction errors ($CL_e^{\pm}$) using the expression given in (12).

$$CL_e^{\pm} = \mu_e \pm Z_\alpha \times S_e \quad (12)$$

In this calculation, μ_e represents the average of the prediction errors ($\mu_e = \sum_{j=1}^{N} e_j$), while S_e is their standard deviation, defined as $S_e = \sqrt{\frac{(\mu_j - \mu_e)^2}{N-1}}$. The term Z_α corresponds to the standard normal value at a chosen significance level α%. The sign of μ_e gives insight into the model's tendency: a positive μe suggests that the model underestimates predictions, whereas a negative μe indicates overestimation. To make a fair comparison of the uncertainty among the models developed in this study, the $CL_e^{\pm}$ values at a 5% significance level for the testing stages are summarized in Table (5).

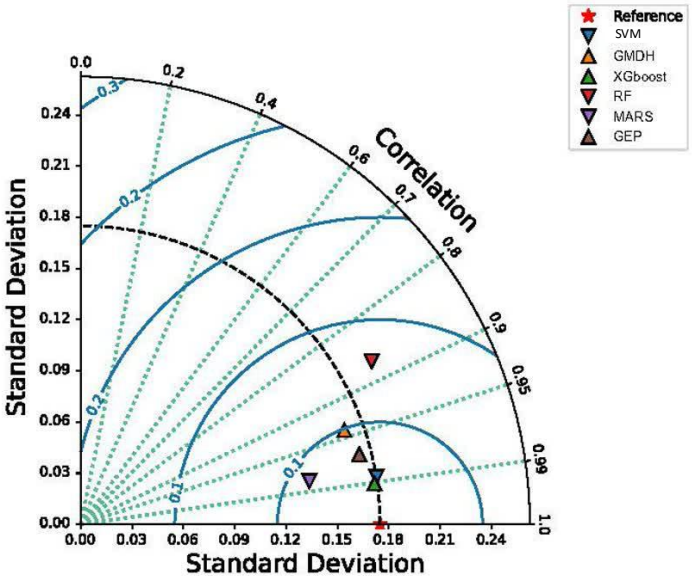


Fig 15- Taylor diagram for SVM, RF, GEP, GMDH, MARS and XGBoost models

Table 5- Uncertainty analysis parameters for different ML models

Predictive model	μe	Se	$CL^{+}e$	$CL^{-}e$	Uncertainty Band ($CL^{+}e$ - $CL^{-}e$)
MARS	0.000332	0.018748	0.001734	-0.00107	0.002804
GEP	0.003497	0.029559	0.005708	0.001287	0.004421
XGBOOST	-0.00118	0.016066	2.42E-05	-0.00238	0.002403

The uncertainty analysis results show that the GEP and MARS models exhibit positive mean errors (μe), indicating a tendency to underestimate the predicted Q*, whereas the XGBoost model, with a negative μe, tends to overestimate Q*. In terms of prediction uncertainty, the XGBoost model demonstrates the lowest uncertainty band (0.002403), followed by MARS (0.002804) and GEP (0.004421), suggesting that XGBoost provides the most stable predictions with minimal variability in error bounds. This finding aligns with the performance metrics, confirming that the XGBoost model exhibits superior predictive reliability compared with the other models developed in this study.

Conclusions

This study evaluated the capability of three advanced data-driven models—Multivariate Adaptive Regression Splines (MARS), Extreme Gradient Boosting (XGBoost), and Gene Expression Programming (GEP)—to predict the dimensionless discharge capacity (Q*) of rectangular top-hinged flap gates (RTHGs) operating under free-flow conditions. The models were developed using a comprehensive laboratory dataset and a set of hydraulically meaningful dimensionless parameters derived from dimensional analysis. Model performance was assessed through multiple statistical criteria and graphical diagnostics to ensure a robust and objective comparison.

Among the investigated approaches, the MARS model demonstrated the highest predictive accuracy, yielding the lowest RMSE (0.00578) and MAE (0.00818), along with the highest coefficient of determination (R^2 = 0.9978). This superior performance confirms the ability of the spline-based MARS structure to effectively capture complex nonlinear interactions between hydraulic and geometric variables governing flap-gate discharge. The XGBoost model ranked second, exhibiting strong predictive capability (R^2 = 0.9877) and high numerical stability, while the GEP model—despite providing explicit analytical equations—showed relatively lower accuracy. Overall, the results indicate that modern machine learning techniques, particularly MARS and

XGBoost, significantly outperform traditional empirical or regression-based equations in estimating flap-gate discharge capacity.

Comparisons with previously published formulations and data-driven studies further confirmed the superior performance of the proposed models. Sensitivity analysis and SHAP interpretation revealed that the relative upstream water depth (h/B) is the most influential parameter affecting Q*, which is consistent with established hydraulic theory. In addition, gamma test results supported the selection of optimal input combinations by reducing model noise and enhancing smoothness.

It is acknowledged that reliance on a single experimental dataset limits claims of universal applicability. However, for the present objective—demonstrating the effectiveness of MARS, XGBoost, and GEP models for RTHG discharge prediction—the selected dataset offers an optimal balance of experimental rigor, parametric coverage, and internal consistency. Future studies should validate the proposed models using independent laboratory datasets, incorporate field measurements from operational flap-gate installations, and extend the framework to include additional gate geometries and submergence effects.

Overall, this study highlights the strong potential of integrating advanced machine learning techniques with hydraulic modeling to develop accurate, robust, and cost-effective predictive tools for flow measurement structures in irrigation and hydraulic engineering applications.

Conflict of Interest

The authors declared no potential conflicts of interest concerning the research, authorship, and publication of this article. Confirmation

Funding

The authors received no financial support for the research, authorship, and publication of this article.

Data Availability Statements

The datasets generated and/or analyzed during the current study are available from the corresponding author on reasonable request.

Ethical considerations

The authors avoided data fabrication, falsification, and plagiarism, and any form of misconduct.

Declaration of Generative AI and AI-assisted technologies in the writing process

The authors state that they have not used generative AI or AI-assisted technologies in their manuscript.

Authors' contribution

First Author: Bahare Behdarvandi, Investigation, Methodology, Visualization.
Second Author: Mohammadreza Zayeri, Conceptualization, Software, Formal analysis, Writing – original draft, Writing – review & editing, Supervision, Project administration.
Third Author: Mehdi Ghomeshi, Data curation, Investigation, Validation, Writing – review & editing.
Fourth author: Mehdi Daryaee, Validation, Resources, Supervision, Writing – review & editing.

References

1- Afaridegan, E., Amanian, N. and Goodarzi, M.R., 2025a. Hybrid machine learning models for discharge coefficient prediction in hydrofoil-crested stepped spillways. *Archives of Computational Methods in Engineering*, *32*(7), pp.4413-4445. https://doi.org/10.1007/s11831-025-10274-z.

2- Afaridegan, E., Fatahi-Alkouhi, R., Khalilian, S., Moradi-Eshgafti, A. and Amanian, N., 2025b. Enhanced energy dissipation prediction in modified semi-cylindrical weirs using machine learning techniques. *Modeling Earth Systems and Environment*, *11*(2), p.131. https://doi.org/10.1007/s40808-025-02317-y.

3- Agalbjorn, S., Koncar, N. and Jones, A.J., 1997. A note on the gamma test. *Neural Comput Appl*, *5*(3), pp.131-133.

4- Asgharzadeh-Bonab, A., Bijanvand, S., Parsaie, A. and Afaridegan, E., 2025. Machine learning-based estimation of discharge coefficient for semicircular labyrinth weirs. *Scientific Reports*, *15*(1), p.33002. https://doi.org/10.1038/s41598-025-18230-4

5- Behdarvandi, B., Zayeri, M.R., Ghomeshi, M. and Daryaee, M., 2024. Performance of Support Vector Machines, Random Forest, and GMDH Methods for Predicting Flow Rate from Rectangular Flap Gates. *Irrigation and Water Engineering*, *15*(2), pp.1-20. https://doi.org/10.22125/iwe.2024.460044.1811

6- Belaabed, F., Arabet, L., Goudjil, K. and Ouamane, A., 2025. Optimized machine learning models for accurate prediction of the discharge coefficient in hydraulic weirs. *Journal of Hydrology and Hydromechanics*, *73*(3), pp.295-309.https://doi.org/10.2478/johh-2025-0023

7- Bijanvand, S., Asgharzadeh-Bonab, A., Parsaie, A., Afaridegan, E., 2025. Enhanced prediction of discharge coefficients in Harmonic Plan Circular Weirs using advanced machine learning and ensemble techniques. *Flow Measurement and Instrumentation* 102, 102812.

8- Chuzhanova, N.A., Jones, A.J. and Margetts, S., 1998. Feature selection for genetic sequence classification. *Bioinformatics (Oxford, England)*, *14*(2), pp.139-143. https://doi.org/10.1093/bioinformatics/14.2.139.

9- De Oliveira, M.C., 1999. Linear systems control design based on linear matrix inequalities (Ph. D. thesis). *Campinas, SP, Brazil: University of Campinas* (in Portuguese).

10- Ferreira, C., 2006. Designing Neural Networks Using Gene Expression Programming, in: Abraham, A., De Baets, B., Köppen, M., Nickolay, B. (Eds.), Applied Soft Computing Technologies: The Challenge of Complexity, Advances in Soft Computing. Springer-Verlag, Berlin/Heidelberg, pp. 517–535. https://doi.org/10.1007/3-540-31662-0_40

11- Ferreira, C., 2001. Gene expression programming: a new adaptive algorithm for solving problems. *arXiv preprint cs/0102027*. https://doi.org/10.48550/arXiv.cs/0102027.

12- Friedman, J.H., 1991. Multivariate adaptive regression splines. *The annals of statistics*, *19*(1), pp.1-67. https://doi.org/10.1214/aos/1176347963

13- Gorgin, F., Vatankhah, A.R., 2022. Rectangular top-hinged plate as portable flow measuring device. *Water Supply* 22, 8637–8658. https://doi.org/10.2166/ws.2022.400

14- Han, Y., Wu, J., Zhai, B., Pan, Y., Huang, G., Wu, L., Zeng, W., 2019. Coupling a Bat Algorithm with XGBoost to Estimate Reference Evapotranspiration in the Arid and Semiarid Regions of China. Advances in Meteorology 2019, 1–16. https://doi.org/10.1155/2019/9575782

15- Hassan, M., Ali Shamim, M., Sikandar, A., Mehmood, I., Ahmed, I., Ashiq, S.Z., Khitab, A., 2015. Development of sediment load estimation models by using artificial neural networking techniques. Environ Monit Assess 187, 686. https://doi.org/10.1007/s10661-015-4866-y

16- Koncar, N., 1997. *Optimisation methodologies for direct inverse neurocontrol* (Doctoral dissertation, University of London).

17- Litrico, X., Belaud, G., Baume, J.-P., Ribot-Bruno, J., 2005. Hydraulic Modeling of an Automatic Upstream Water-Level Control Gate. *Journal of Irrigation and Drainage Engineering* 131, 176–189. https://doi.org/10.1061/(ASCE)0733-9437(2005)131:2(176)

18- Lundberg, S.M. and Lee, S.I., 2017. A unified approach to interpreting model predictions. *Advances in neural information processing systems*, *30*.

19- Mahmoudi, B., Farhoudi, J., 2019. Discharge estimation of flap gate installed in a circular channel under free flow condition. Iranian Water Researches Journal 13(1), 127–136.

20- Moghaddamnia, A., Remesan, R., Kashani, M.H., Mohammadi, M., Han, D. and Piri, J., 2009. Comparison of LLR, MLP, Elman, NNARX and ANFIS Models—with a case study in solar radiation estimation. *Journal of Atmospheric and Solar-Terrestrial Physics*, *71*(8-9), pp.975-982. 10.1016/j.jastp.2009.04.009.

21- Moghtaderi, A., Valizadegan, E., 2021. Investigation of the hydraulic characteristics of flap gates at the end of trapezoidal channels.

22- Nejatipour, P., Oliveto, G., Sapaev, I., Afaridegan, E. and Fatahi-Alkouhi, R., 2025. Prediction and uncertainty quantification of flow rate through rectangular top-hinged gate using hybrid gradient boosting models. *Water*, *17*(24), p.3470. https://doi.org/10.3390/w17243470

23- Parsa, A.B., Movahedi, A., Taghipour, H., Derrible, S. and Mohammadian, A.K., 2020. Toward safer highways, application of XGBoost and SHAP for real-time accident detection and feature analysis. *Accident Analysis & Prevention*, *136*, p.105405. Doi: 10.1016/j.aap.2019.105405.

24- Piri, J., Amin, S., Moghaddamnia, A., Keshavarz, A., Han, D. and Remesan, R., 2009. Daily pan evaporation modeling in a hot and dry climate. *Journal of Hydrologic Engineering*, *14*(8), pp.803-811.https://doi.org/10.1061/(ASCE)HE.1943-5584.0000056

25- Remesan, R., Shamim, M.A. and Han, D., 2008. Model data selection using gamma test for daily solar radiation estimation. *Hydrological processes*, *22*(21), pp.4301-4309.https://doi.org/10.1002/hyp.7044

26- Remesan, R., Shamim, M.A., Han, D. and Mathew, J., 2009. Runoff prediction using an integrated hybrid modelling scheme. *Journal of Hydrology*, *372*(1-4), pp.48-60. DOI: 10.1016/j.jhydrol.2009.03.034.

27- Salehi, S. and Azimi, A.H., 2019. Discharge characteristics of weir-orifice and weir-gate structures. *Journal of Irrigation and Drainage Engineering*, *145*(11), p.04019025.https://doi.org/10.1061/(ASCE)IR.1943-4774.0001421

28- Salmasi, F., Shadkani, S., Abraham, J. and Malekzadeh, F., 2022. Experimental investigation for determination of discharge coefficients for inclined slide gates and comparison with data-driven models. *Iranian Journal of Science and Technology, Transactions of Civil Engineering*, *46*(3), pp.2495-2509.https://doi.org/10.1007/s40996-022-00850-9

29- Shamim, M.A., Remesan, R., Bray, M. and Han, D., 2015. An improved technique for global solar radiation estimation using numerical weather prediction. *Journal of Atmospheric and Solar-Terrestrial Physics*, *129*, pp.13-22. DOI: 10.1016/j.jastp.2015.03.011.

30- Stefánsson, A., Končar, N. and Jones, A.J., 1997. A note on the gamma test. *Neural Computing & Applications*, *5*(3), pp.131-133.https://doi.org/10.1007/BF01413858.

31- Valipour, M., 2013. Increasing irrigation efficiency by management strategies: cutback and surge irrigation.

32- Yan, X., Wang, Y., Fan, B., Mohammadian, A., Liu, J. and Zhu, Z., 2023. Data-driven modeling of sluice gate flows using a convolutional neural network. *Journal of Hydroinformatics*, *25*(5), pp.1629-1647. https://doi.org/10.2166/hydro.2023.200.

33- Zhang, W., 2020. MARS Applications in Geotechnical Engineering Systems: Multi-Dimension with Big Data. *Springer Singapore*, Singapore. https://doi.org/10.1007/978-981-13-7422-7.